

000
001
002
003
004
005
006
007
008
009
010
011
012
013
014
015
016
017
018
019
020
021
022
023
024
025
026
027
028
029
030
031
032
033
034
035
036
037
038
039
040
041
042
043
044
045
046
047
048
049
050
051
052
053

054
055
056
057
058
059
060
061
062
063
064
065
066
067
068
069
070
071
072
073
074
075
076
077
078
079
080
081
082
083
084
085
086
087
088
089
090
091
092
093
094
095
096
097
098
099
100
101
102
103
104
105
106
107

Deep Manifold Prior

Anonymous ICCV submission

Paper ID —

Abstract

We present a prior for manifold structured data, such as surfaces of 3D shapes, where deep neural networks are adopted to reconstruct a target shape using gradient descent starting from a random initialization. We show that surfaces generated this way are smooth, with limiting behavior characterized by Gaussian processes, and we mathematically derive such properties for fully-connected as well as convolutional networks. We demonstrate our method in a variety of manifold reconstruction applications, such as point cloud denoising and interpolation, achieving considerably better results against competitive baselines while requiring no training data. We also show that when training data is available, our method allows developing alternate parametrizations of surfaces under the framework of AtlasNet [14], leading to a compact network architecture and better reconstruction results on standard image to shape reconstruction benchmarks.

1. Introduction

In recent years a variety of approaches have been proposed to generate manifold data such as surfaces of 3D shapes using deep networks. The goal of this work is to characterize how the choice of the network architecture impacts the properties of the resulting surfaces. We present a *deep manifold prior*, an approach to represent a manifold as a collection of transformations (atlas) of an Euclidean space parameterized using deep networks (Section 3). We show that random networks induce smooth surfaces whose limiting behavior can be understood in terms of a Gaussian process (GP) [6, 21, 37]. We derive the mean and covariance function of the surface coordinates, and in some cases of the surface normal and curvature, as a function of network architecture (Section 4). Our analysis can also be used to derive the properties of surfaces induced by the level-set of a scalar field, $f(x) = c$, parameterized using a deep network.

As a concrete application we study the problem of interpolating and denoising point clouds sampled from contours or surfaces of shapes, as seen in Figures 1 and 2.

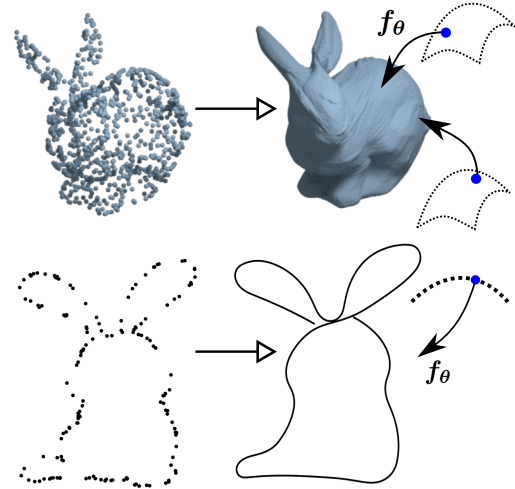


Figure 1: **The deep manifold prior.** Points interpolated using deep networks to map points in a 2D grid (top) and 1D grid (bottom) to the target shape (a 3D surface and a 2D curve respectively). The networks are randomly initialized and trained to minimize the Chamfer distance to the target.

The manifold parametrization allows us to efficiently sample point clouds, which can be combined with a Chamfer metric to measure a reconstruction error with respect to the sampled data. We show that smooth surfaces are obtained when the parameters of the networks are learned to minimize the reconstruction error starting from a *random initialization* (Figure 2). The approach is also effective for the level-set formulation, where the objective is to learn a deep network that correctly classifies points as *inside* or *outside* the surface. However, an advantage of the explicit parametrization is that it does not require the notion of what is inside. In addition we introduce a *regularization* that reduces self-intersections, overlaps, and distortion of the parametrization, which is desirable for applications such as texture mapping (Section 3). Our approach requires *no* prior learning, works across a range of 3D shapes, and outperforms strong baselines for point cloud denoising, such as Screened Poisson Surface Reconstruction (SPSR) and Robust Implicit Moving Least Squares (RIMLS). It is also more lightweight than approaches that operate on vol-

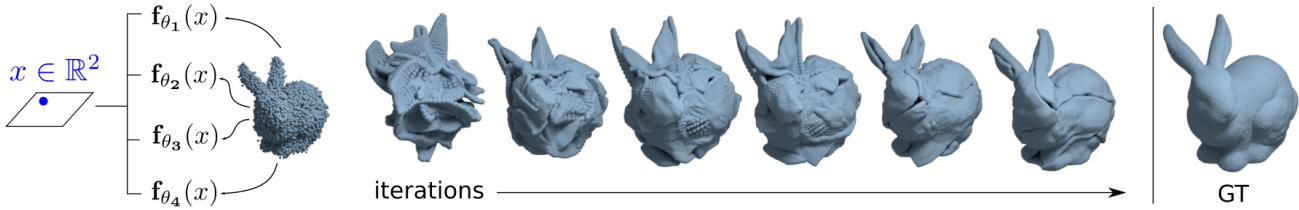


Figure 2: **Manifold reconstruction pipeline.** Manifold parametrizations are encoded by neural networks (f_{θ_i}) and trained to minimize the reconstruction error with respect to the noisy target (left). Prior induced by the neural networks makes the generated surface much closer to the ground-truth (right), without ever seeing any additional training data.

umetric representations of 3D shapes (Section 5).

Our analysis sheds lights on the impressive performance of several recently proposed architectures for 3D surface generation, such as MRTNet [12], AtlasNet [14], FoldingNet [40], and Pixel2Mesh [36], as well as implicit surface approaches [4, 13, 20, 24]. These can be interpreted as different ways of parameterizing a manifold. In particular, AtlasNet generates a 3D shape as a collection of surfaces, each represented as a transformation of a unit grid using a fully-connected network. However, the generated pieces exhibit significant overlap which results in a poor surface reconstruction and is less desirable for applying materials and textures to the surface (Section 5). The proposed regularization alleviates this problem. Moreover, by replacing the fully-connected networks of AtlasNet with convolutional variants we improve the performance on standard benchmarks for shape generation [7] with networks that have a fraction of the parameters, faster inference time, as well as smaller memory footprint (Section 5).

2. Related Work

Manifold 3D shape generation 3D shape generation is an active area of research with methods that generate 3D shapes as volumetric representations such as occupancy grids [7, 11, 15, 25, 32, 34, 39], signed distance functions [4, 13, 20, 24], multiview depth and normals [18, 19, 29, 31], or point clouds [1, 9, 10, 12]. Our work is closely related to techniques for generating 3D shapes through a predefined connectivity or parametrization structure over the surface of the shape. Pixel2Mesh [36] utilizes graph convolutional networks to generate meshes that are homeomorphic to a sphere. AtlasNet [14] and FoldingNet [40] learn a parametrization of a surface by adopting deep networks to transform point coordinates in a 2D plane to the shape surface. Specifically, each point is generated as $(f_{\theta}^1(x), f_{\theta}^2(x), f_{\theta}^3(x))$ where f_{θ}^i is a deep network and $x = (x_1, x_2)$ is a point in the unit grid. Alternate approaches [4, 13, 20, 24] represent the surface as the level-set of a scalar field, $f(x) = 0, x \in \mathbb{R}^3$, e.g., of the signed distance function. While these have been applied for shape generation by training on 3D shape datasets, our goal is to

analyze the role of these parameterizations as an *implicit prior* for manifold denoising and interpolation tasks.

Deep implicit priors Our work is related to the deep image prior [35] that generates images as a convolutional network transformation of a random signal on a unit grid. By optimizing the randomly initialized network to minimize a reconstruction loss with respect to the noisy target, their approach was shown to yield excellent denoising results. Our approach generalizes this idea to manifold data, which is more appropriate for interpolating and denoising contours and surfaces (see Figure 6 for a comparison). Our work is also related to the recently proposed deep geometric prior [38]. Their approach was used to estimate a surface from point cloud data by partitioning the surface into small overlapping patches and reconstructing the local manifold using a deep network. Consistency in the overlapping regions was enforced by minimizing the Earth Movers distance (EMD). In contrast to their work, we learn a small collection of non-overlapping parametrizations (atlas) by minimizing a regularized term and Chamfer distance, which is much more efficient than EMD. We also consider diverse tasks such as point cloud denoising, interpolation, and shape reconstruction across a category where the atlases needs to be consistent across instances. Finally, we present a theoretical analysis of the local properties of the generated surface by analyzing its limiting behavior as a Gaussian process.

Embedding a manifold Our work is related to techniques for embedding manifolds into a low-dimensional Euclidean space (e.g., IsoMap [33] or LLE [26]). Our approach parameterizes the inverse mapping from the Euclidean space to the data manifold using a deep network. Interestingly, invertability can be guaranteed by using networks with easy to compute inverses (e.g., NICE [8] or GLOW [17]). In computer graphics, a number of techniques have been developed for shape surface denoising and reconstruction. Screened Poisson Reconstruction [16] constructs an implicit surface on a 3D volumetric grid based on oriented point samples by solving the Poisson equation. Approaches based on Moving Least Squares [2, 23, 27] reconstruct a surface by estimating

an approximation of each local patch, similar to the deep geometric prior [38] approach. Our approach outperforms these baselines by a significant margin (Table 1).

Deep networks and Gaussian processes A Gaussian process (GP) is commonly viewed as a prior over functions. Let T be an index set (e.g., $T \in \mathbb{R}^d$), let $\mu(t)$ be a real-valued mean function and $K(t, t')$ be a non-negative definite kernel or covariance function on T . If $f \sim GP(\mu, K)$, then, for any finite number of indices $t_1, \dots, t_n \in T$, the vector $(f(t_i))_{i=1}^n$ is Gaussian distributed with mean vector $(\mu(t_i))_{i=1}^n$ and covariance matrix $(K(t_i, t_j))_{i,j=1}^n$. Neal [21] showed that a two-layer network with infinite number of hidden units approaches a GP. The mean and covariance of commonly used non-linearities have been derived in several subsequent works [6, 37]. We use this machinery to analyze the limiting GP of deep manifold priors.

3. Method

Background Our focus is to define priors over *manifolds*. We first introduce some basic notation. A n -*manifold* is a topological space \mathcal{M} for which every point in \mathcal{M} has a neighborhood homeomorphic to the Euclidean space \mathbb{R}^n . Let $\mathcal{U} \subset \mathcal{M}$ and $\mathcal{V} \subset \mathbb{R}^n$ be open sets. A homeomorphism $\phi : \mathcal{U} \rightarrow \mathcal{V}$, $\phi(u) = (x_1(u), x_2(u), \dots, x_n(u))$ is a *coordinate system* on \mathcal{U} and x_1, x_2, \dots, x_n are *coordinate functions*. The pair $\langle \mathcal{U}, \phi \rangle$ is a *chart*, whereas $\zeta = \phi^{-1}$ is a *parameterization* of \mathcal{U} . An *atlas* on \mathcal{M} is a collection of charts $\{\mathcal{U}_\alpha, \phi_\alpha\}$ whose union covers \mathcal{M} . Intuitively, surfaces are 2-manifolds where as contours are 1-manifolds. Thus the dimensionality of the input of the parameterization or the output of the chart corresponds to the order n of the manifold. Atlases can be used to represent manifolds that cannot be decomposed using a single parametrization (e.g., the surface of a sphere can be diffeomorphically mapped to two planes but not one.)

General framework In our work we will replace the search over \mathcal{U} by a search over the parameters θ of the DNN f_θ that encodes the parameterization $f_\theta = \zeta = \phi^{-1}$. More specifically, given a set of points $P \in \mathcal{M}$, we aim to recover the manifold \mathcal{M} by computing the following:

$$\theta^* = \arg \min_{\theta} \mathcal{L}_C(f_{\theta, x \sim \mathbb{R}^n}(x), P). \quad (1)$$

The approximated manifold can then be reconstructed in the domain on which it is embedded f_{θ^*} . In practice, we restrict x to the unit hypercube $[0, 1]^n$. Here \mathcal{L} is a loss function that computes a discrepancy between sets. Thus, reconstructing a manifold represented by an atlas of k charts is done by

computing the following:

$$\theta_1^*, \theta_2^*, \dots, \theta_k^* = \arg \min_{\theta_1, \theta_2, \dots, \theta_k} \mathcal{L}_C\left(\bigcup_{i=1}^k f_{\theta_i}(x), P\right) \quad (2)$$

Parameterization We explore two choices of parameterizations of the coordinate function $f_\theta(x)$ as a deep neural network. The first uses a multi-layer perception (MLP) to represent the parameterization explicitly: the network receives as an input a value $x \in \mathbb{R}^n$ and outputs the coordinates of point in the manifold. We use ReLU non-linearities throughout the network, except for the last layer where we use tanh. This representation is analogous to the ones used in [14, 40]. The second choice is to encode \mathcal{M} directly through a convolutional network $g(z)$, where z is a stationary signal (Gaussian noise). We use 2D convolutional layers followed by ReLU activations and bilinear upsampling, except for the last layer where we use tanh. The convolutional parametrization induces a stationary prior (see Supplementary for details), and we observe the resulting architectures are more memory-efficient and compact than the first choice.

Loss function A key part of our method is computing a distance between two sets of points P_1 and P_2 . Such distance metric needs to be differentiable and reasonably efficient to compute, since the cardinality of the sets might be large. Thus, similarly to previous work [12, 14, 36, 40], we employ the Chamfer distance \mathcal{L}_C defined as follows:

$$\mathcal{L}_C(P_1, P_2) = \sum_{p_1 \in P_1} \min_{p_2 \in P_2} \|p_1 - p_2\|_2^2 + \sum_{p_2 \in P_2} \min_{p_1 \in P_1} \|p_1 - p_2\|_2^2.$$

Stretch regularization Representing the manifold as a set of multiple parameterizations output by DNNs has some drawbacks. First, there is no guarantee that the charts are invertible, which means that a surface generated by f_θ might contain self-intersections. Second, multiple charts might be representing the same region of the manifold. In theory this is not a problem as long as overlapping regions are consistent. However, in practice this consistency is hard to achieve when point clouds are sparse and noisy. We propose to alleviate those issues by penalizing the stretch of the computed parameterization. Let $\mathcal{N}(w)$ be the neighborhood of w in \mathbb{R}^n , the *stretch regularization* \mathcal{L}_S can be defined as follows:

$$\mathcal{L}_S(\theta) = \mathbb{E}_{x \sim [0,1]^n} \left[\sum_{x' \in \mathcal{N}(x)} \|f_\theta(x) - f_\theta(x')\|_2^2 \right]. \quad (3)$$

Notice that we can compute the neighbors of x ahead of time which makes the computation significantly cheaper. In practice, we sample x from a set of predefined regularly

spaced values in $[0, 1]$ – a regular grid in the 2D case. Now we can define our full loss function as follows.

$$\mathcal{L}(\theta) = \mathcal{L}_C(\mathbf{f}_\theta, x \sim \mathbb{R}^n(x), P) + \lambda \mathcal{L}_S(\theta), \quad (4)$$

where $\theta = \theta_1, \theta_2, \dots, \theta_k$ and $\mathbf{f}_\theta(x) = \bigcup_{i=1}^k f_{\theta_i}(x)$.

Manifolds as deep level-sets An alternative approach is to represent d -manifold as the level-set of a scalar function over $d + 1$ dimensions. For example, a surface can be represented as the level set, $f(x) = 0$, where $x \in \mathbb{R}^3$. Prior work [4, 13, 20, 24] has explored this approach to generate a 3D surface by approximating its signed distance function. Level-set formulation can naturally handle shapes with different topologies, but require the knowledge of what is inside the surface, which can be challenging to estimate for imperfect point-cloud data. In this work, we also characterize and experiment with the manifold prior induced by the level-set of a deep network $f_\theta(x) = 0$ initialized randomly.

4. Limiting GP for the Deep Manifold Prior

Consider the case when the manifold coordinates are parameterized using a deep network $f_\theta(x)$. We show that random networks, *e.g.*, whose parameters are drawn i.i.d. from a Gaussian distribution, produces smooth manifolds. This is done by analyzing the limiting behavior of the function as a Gaussian process. In practice this is a good approximation to networks that are relatively shallow and have hundreds of hidden units in each layer.

Concretely, the mean $\mathbb{E}_\theta[f_\theta(x)]$ and covariance $\mathbb{E}_\theta[f_\theta(x)f_\theta(y)^T]$ of the parameterization characterize the structure of the generated manifold. For example, the covariance function of a smooth manifold decays slowly as a function of distance in the input space compared to a rough one. Following prior work [6, 21, 37], we first derive the mean and covariance for a two layer network with a scalar output. We then generalize the analysis to vector outputs and multi-layer networks.

Consider a two-layer fully-connected network on an input $x \in \mathbb{R}^n$. Let H be the number of units in the hidden layer represented using parameters $U = (u_1, u_2, \dots, u_H)$ where $u_j \in \mathbb{R}^n$ and the second layer has one output parameterized by weights $v \in \mathbb{R}^H$. Denote the non-linearity applied to each unit as the scalar function $h(\cdot)$. The output of the network is: $f(x) = \sum_{k=1}^H v_k h(u_k^T x)$. When the parameters U and v are drawn from a Gaussian distributions $N(0, \sigma_u^2 \mathbb{I})$ and $N(0, \sigma_v^2 \mathbb{I})$ respectively, we have:

$$\mathbb{E}_{U,v}[f(x)] = \mathbb{E}_{U,v} \left[\sum_{k=1}^H v_k h(u_k^T x) \right] = 0,$$

since U and v are independent and zero mean. Similarly, the covariance function $K(x, y)$ can be shown to be:

$$K(x, y) = \mathbb{E}_{U,v}[f(x)f(y)] = H\sigma_v^2 \mathbb{E}_U [h(u_k^T x) h(u_k^T y)].$$

This follows since each u_k is drawn i.i.d, each v_k is independent and drawn identically from a Gaussian distribution with zero mean. The quantity $V(x, y) = \mathbb{E}_u [h(u^T x)h(u^T y)]$ can be computed analytically for various transfer functions. Williams [37] showed that when $h(t) = \text{erf}(t) = 2/\sqrt{\pi} \int_0^t e^{-t^2} dt$, then

$$V_{\text{erf}}(x, y) = \frac{2}{\pi} \sin^{-1} \frac{x^T \Sigma y}{\sqrt{(x^T \Sigma x)(y^T \Sigma y)}}. \quad (5)$$

Here $\Sigma = \sigma^2 \mathbb{I}$ is the covariance of u . For the ReLU non-linearity $h(t) = \max(0, t)$, Cho and Saul [6] derived the expectation as:

$$V_{\text{relu}}(x, y) = \frac{1}{\pi} \|x\| \|y\| (\sin \psi + (\pi - \psi) \cos \psi), \quad (6)$$

where $\psi = \cos^{-1} \left(\frac{x^T y}{\|x\| \|y\|} \right)$. We refer the reader to [6, 37] for kernels corresponding of other transfer functions.

An application of the Central Limit Theorem shows that by letting σ_v^2 scale as $1/H$ and $H \rightarrow \infty$, the output of a two layer convolutional network converges to a Gaussian distribution with zero mean and covariance

$$K_1(x, y) = \mathbb{E}_{U,v}[f(x)f(y)] = V(x, y). \quad (7)$$

Hence the limiting behavior of the DNN can be approximated as a Gaussian process with a zero mean and covariance function $K(x, y) = V(x, y)$.

Extending to multiple outputs The above analysis can be extended to the case when the function $f(x)$ is vector valued. For example a 2-manifold in 3D can be represented as $f(x) = (f^1(x), f^2(x), f^3(x))$, with $x \in \mathbb{R}^2$. In our case, the functions share a common backbone and each $f^i(x)$ is constructed from the outputs of the last hidden layer parameterized with weights v^i , *i.e.*, $f^i(x) = \sum_{k=1}^H v_k^i h(u_k^T x)$. From the earlier analysis we have that each $f^i(x)$ has zero mean in expectation. And the covariance between dimension i and j of f is:

$$K_1^{i,j}(x, y) = \mathbb{E}_{U,v_i,v_j} [f^i(x)f^j(y)] = V(x, y) \mathbf{1}[i = j].$$

This follows from the fact that each v_k^i is independent and drawn from a zero mean distribution. Thus, the covariance is a diagonal matrix with entries $V(x, y)$ in its diagonal.

Extending to multiple layers The analysis can be extended to multiple layers by recursively applying the formula for the two-layer network. Denote $K_\ell(x, y)$ as the

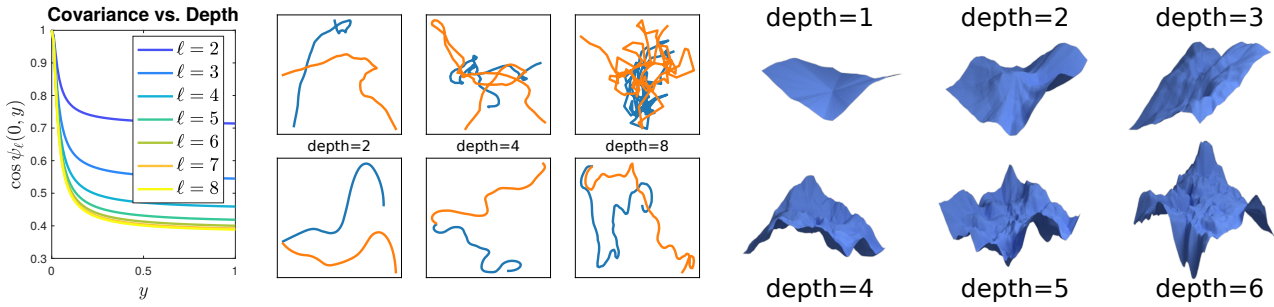


Figure 3: **Characterizing the deep manifold prior.** (left) a plot demonstrating the relationship between the network depth and the covariance function for the limiting GP. (middle) Random curves generated by the coordinate (top rows) and arc-length (bottom rows) parametrizations using deep networks with varying depths. (right) Random surfaces generated by deep networks of varying depths.

covariance function of a scalar valued fully-connected network with $\ell + 1$ layers and $J(\theta) = \sin \theta + (\pi - \theta) \cos \theta$. Following [6] for the ReLU non-linearity we have the following recursion:

$$K_{\ell+1}(x, y) = \frac{1}{\pi} (K_{\ell}(x, x)K_{\ell}(y, y))^{1/2} J(\psi_{\ell}).$$

Where $\psi_{\ell}(x, y) = \cos^{-1} \frac{K_{\ell}(x, y)}{\sqrt{K_{\ell}(x, x)K_{\ell}(y, y)}}$ and $K_0(x, y) = x^T y$. Note that if in each layer we add a bias term sampled from a $N(0, \sigma_b^2)$ the covariance changes to $K_{\ell}(x, y) + \sigma_b^2$ and the mean remains unchanged at zero.

4.1. Discussion and Analysis

The above analysis shows that random networks induce certain priors over the coordinates of the manifold. The effect of increasing the depth of the network can be seen by visualizing how the covariance $\cos \psi_{\ell}(x, y)$ varies as a function of depth. Figure 3 plots $\cos \psi_{\ell}(x, y)$ at $x = 0$ for a curve as a function of the depth of the network for $\sigma_b = 0.01$. The covariance decays faster with depth, indicating that the deeper networks produce manifolds with higher spatial frequencies (or curvatures). This can also be seen in Figure 3 which shows random curves (middle) from a surfaces (right) for networks with varying depths.

One potential drawback of fully-connected network parameterization is that the generated manifold does not have a stationary (translationally invariant) covariance function. A covariance function $K(x, y)$ is stationary if it can be written as $K(x, y) = k(x - y)$. On the other hand, a convolutional network that produces coordinates through a series of convolutional layers operating on a random noise has a stationary covariance [5]. This is identical to the approach for generating natural images in the deep image prior [35] and we explore this alternative in Section 5.2.

Normals and curvature While we have shown that the outputs $f(x)$ induced by random networks is a GP in

the limit, what can be said about intrinsic properties such as normals and curvature? Consider the curve $\gamma(t) = (x(t), y(t))$. Since derivatives are linear operators, it follows that distribution of derivatives, \dot{x} and \dot{y} , are also Gaussian [28]. The curvature is given by $\kappa = (\dot{x}\dot{y} - \dot{y}\dot{x})/(\dot{x}^2 + \dot{y}^2)^{3/2}$. Unfortunately, since each of the derivatives converge to a zero mean Gaussian distribution, the limiting distribution of the curvature κ does not exist. The pathology arises because the parameterization has a speed ambiguity, *i.e.*, replacing t with any monotonic function of t results in the same curve. To avoid this one can directly parametrize the derivatives as $\dot{x} = \cos(f(t))$ and $\dot{y} = \sin(f(t))$ where f is a deep network. This is an arc-length (unit speed) parameterization since $\dot{x}^2 + \dot{y}^2 = 1$. Once the derivatives are generated, the curve can be reconstructed by integration, *i.e.*, $x = \int_0^t \cos(f(t))dt$. In this case the limiting distribution of the coordinates, normal, and curvature all exist and are also GPs. We derive the mean and covariance function in the Supplementary material. Figure 3-middle shows draws from the GP with direct (top) and arc-length (bottom) parametrizations. One can see that arc-length parametrizations lead to more length-uniform curves.

Unlike curves, it is much more challenging to design arc-length parametrizations of surfaces. The difficulty arises due to the fact the gradients need to satisfy additional constraints for the surface to be integrable [30]. Hence, we directly parameterized the coordinate function and proposed the stretch regularization to minimize distortion. Alternatives ways of parameterizing the surface to satisfy properties such as conformality [22] is left for future work.

Deep level-set prior Finally, the GP analysis applies in a straightforward manner to the level-set formation $f_{\theta}(x) = 0$ where f_{θ} is a ReLU network mapping the 3D position $x \in \mathbb{R}^3$ to a scalar. The induced distribution over the scalar field is a GP for random networks. Since for a differentiable function f with non-zero gradient, the gradient is orthogo-

	Surface	Contour	Implicit	RIMLS [23]	SPSR [16]
bunny	2.71E-04	6.64E-04	5.52E-04	1.43E-03	3.96E-04
dragon	4.18E-04	6.12E-04	1.20E-03	1.65E-03	1.46E-02
car	2.73E-04	4.57E-04	6.83E-02	1.50E-03	2.10E-03
cup	2.59E-04	5.80E-04	2.64E-02	1.74E-03	1.00E-02
mobius	3.51E-04	4.95E-04	3.26E-03	1.96E-03	1.89E-02
chair	3.95E-04	4.22E-04	7.32E-03	2.09E-03	2.58E-02
spiral	1.05E-03	7.31E-04	1.64E-02	2.98E-03	7.90E-02
ring	5.69E-04	5.54E-04	4.81E-02	2.46E-03	3.76E-02
avg.	4.48E-04	5.65E-04	2.13E-02	1.98E-03	2.36E-02

Table 1: **Quantitative results for point cloud denoising.** *Surface*, *Contour* and *Implicit* represent different *deep manifold priors* based on a 2-manifold, 1-manifold and level-set parameterization.

nal to the level set, one can characterize the surface by analyzing the gradient field ∇f . The limiting distribution over the gradient field is also a GP and one can estimate the mean and covariance functions by a similar analysis (see Supplementary material for details). However, the training objective of the level-set prior is different from the explicit parameterization as the network must classify points as inside or outside the surface. This supervision can be challenging to obtain from noisy data, especially for thin structures. We provide a comparison with this approach in Section 5.

5. Experiments

In this section we will present quantitative and qualitative results for applying the manifold prior to multiple manifold reconstruction tasks. All the experiments in this paper were implemented using Python 3.6 and PyTorch. Computation was performed on TitanX GPUs.

5.1. Denoising and Interpolation

Benchmark Our benchmark consists of 8 different 3D shapes with diverse characteristics. The shapes are normalized to fit a unit cube and 16K points are sampled on their surfaces. The point positions are perturbed by a Gaussian noise with standard deviation 2×10^{-3} and zero mean. Figure 7 shows the ground-truth shapes as well as their noisy counterpart. Since the level-set representation and the baseline methods (RIMLS [23], SPSR [16]) require normal information, we estimate the normal for every point by using the local frame defined by its nearest neighbors. We experimented multiple numbers of neighbors for both baselines and used the value that led to the best results: 20 neighbors for SPSR and the level-set representation, 30 neighbors for RIMLS. The network used in the level-set representation follows the same architecture and training protocol as the one used for the explicit parameterizations (described in the next paragraph). However, it is trained to predict every point as outside (+1) or inside the surface (-1). Points with positive values are generated by translating every point in the point cloud along the normal direction for a distance $\epsilon = 2 \times 10^{-3}$. Points with negative values are generated in the same way, but applying a displacement to the opposite

direction. For RIMLS, we used a relative spatial filter size of 10, 15 projection iterations and a volumetric grid with 200^3 resolution. For SPSR, we used an octree with depth 7 and 8 iterations.

Experimental setup Our method performs denoising by minimizing Equation 4. In this framework, P is the noisy point cloud we are trying to reconstruct and f_θ is a neural network. In all experiments we use a neural network with 3 fully connected layers, where the layers have 256, 128 and 64 hidden units, respectively. The output of the networks is a point in \mathbb{R}^3 . The input can be either a point in \mathbb{R} (1-manifold) or \mathbb{R}^2 (2-manifold). We use *ReLU* activations followed by batch normalization at each layer, except for the last, where we use a *tanh* non-linearity. We vary the architecture of f_θ with respect to the number of parameterizations (1 or 8) and dimensionality (1 or 2). Additionally, we try each one of these architectural variations with $\lambda = 0$ and $\lambda = 1.0$. When using 8 parameterizations, 4096 points are sampled per parameterization. When using just one parameterization, 16K points are sampled. We optimize our objective through gradient descent using the Adam optimizer with learning rate 10^{-3} . For evaluation, we uniformly sampled 16K points in the computed manifold (represented as a triangular mesh) and compute the Chamfer distance with respect to the ground-truth.

Results and discussion. Our methods significantly outperform the baselines for most of the shapes. Quantitative results can be seen in Table 1 and the qualitative results are shown in Figure 7. The numbers are computed using 8 parameterizations (for surfaces and curves) and $\lambda = 1.0$. A comparison between different variations of our approach is displayed in Table 2. RIMLS, SPSR and level-set representations (*Implicit* in Table 1) have trouble reconstructing point clouds with a significant amount of noise. This is due to the fact that those methods rely on accurate surface normal estimates to infer inside/outside regions of the shape. Besides, RIMLS and methods based on implicit functions (SPSR and level-set representations) work better when dealing with closed surfaces. Shapes that are better approximated by contours (ring, spiral, chair’s legs) are particularly challenging for those approaches. On the other hand, the networks parametrizing explicit functions (*Surface* and *Contour* in Table 1) are able to adapt to different structures and present a fair performance across a diverse set of shapes.

The results in Table 2 suggest that using multiple parameterizations gives a better approximation than just using a single one. This happens because complex shapes are easier to represent by multiple parameterizations. For example, while using a single 2-manifold parameterization, the ring tends to be approximated by a disk, which significantly increases the reconstruction error when the points are uniformly sampled over the final mesh. This behavior

	S1R	S8R	S1	S8	C1R	C8R	C1	C8	RIMLS [23]	SPSR [16]
avg.	4.48E-03	4.48E-04	2.75E-03	1.35E-03	1.08E-03	5.77E-04	1.00E-03	5.82E-04	1.98E-03	2.36E-02

Table 2: **Ablation studies.** Comparison between different variations of our approach. Naming follows the following convention: S corresponds to a 2-manifold parameterization (surface), whereas C corresponds to a 1-manifold (contour). The following number (1 or 8) corresponds to the number of parameterizations. A R letter is added if stretch regularization was used ($\lambda = 1.0$).

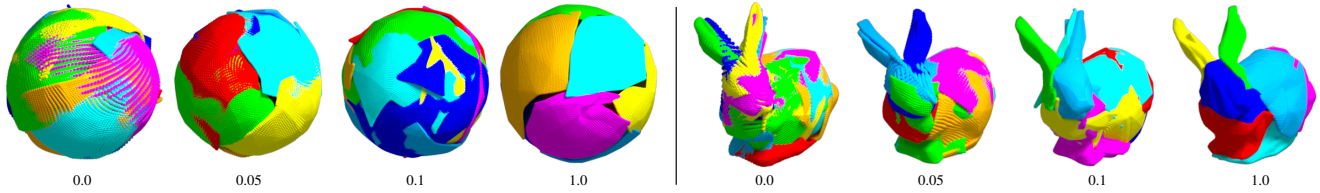


Figure 4: **Effect of the regularization weight on the reconstructed manifold.** For this experiment, we use our method to reconstruct a sphere using an atlas with 8 charts and render each one with a different color. Without any regularization, there is a significant amount of deformation applied to each surface (hence the space between the points) and a considerable amount of overlap between different parts. As the regularization weight increases, those aspects are noticeably reduced.

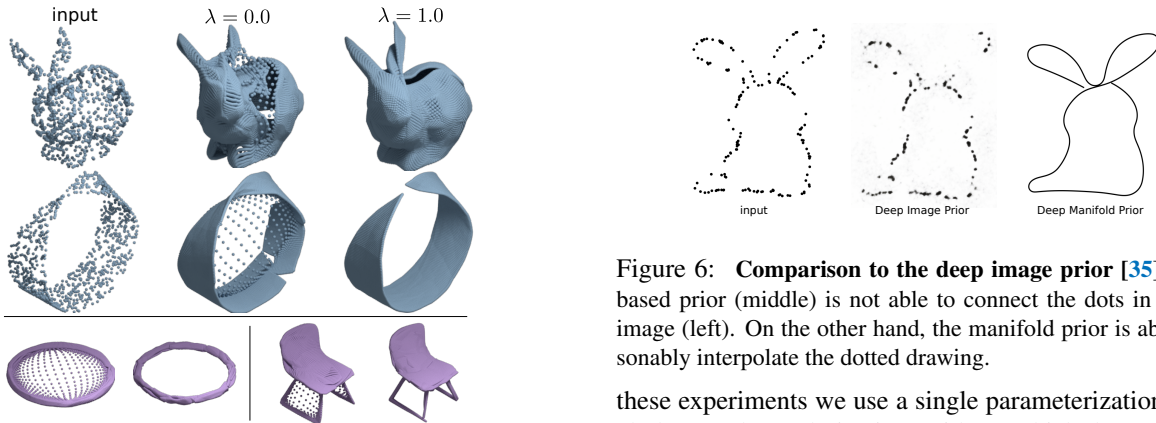


Figure 5: *Interpolation results on the top.* Stretch regularization ($\lambda = 1.0$) helps generate smoother surfaces. *On the bottom, denoising using one vs. multiple parameterizations.* Shapes on the left were reconstructed using a single parameterization, whereas shapes on the right used 8 parameterizations. Using multiple parameterizations helps reconstruct complex shapes.

is illustrated in Figure 5. Our ablation studies also indicate that using stretch regularization helps parameterizations of both surfaces and contours. Figure 4 shows the effect of stretch regularization for two different shapes. As the regularization weight increases, the overlap between different parameterizations becomes smaller. When overlaps exist, the manifold representation is suboptimal – the same regions are being generated multiple times.

Interpolation We also explored using the manifold prior for point cloud interpolation. This experiment follows the same experimental setup as denoising. However, instead of perturbing the points with Gaussian noise, we randomly select 1K points out of 16K. Interpolation is performed by minimizing Equation 4. Results can be seen in Figure 5. For



Figure 6: **Comparison to the deep image prior [35].** Image-based prior (middle) is not able to connect the dots in the input image (left). On the other hand, the manifold prior is able to reasonably interpolate the dotted drawing.

these experiments we use a single parameterization and include stretch regularization, without which the surface has holes and significant folds. Our method is able to reconstruct reasonable surfaces from a small set of points.

Comparison with the deep image prior We also compare our approach to the deep image prior [35] for interpolating points in 2D images. Results are presented in Figure 6. We use the same architecture from [35] while minimizing the mean squared error with respect to the image pixels. For the manifold prior, we use a single 1-manifold parameterization following the architecture described before, differing only in the dimensionality of the output: points in this case are in \mathbb{R}^2 instead of \mathbb{R}^3 . Coordinates of the black pixels in the input image are used to form a point cloud and the manifold is computed by minimizing Chamfer distance with respect to it.

5.2. Learning from data

Finally, we show how the insights presented in the earlier sections, in particular convolutional parameterization and stretch regularization, can also improve generative models of 3D shapes when trained on a large collection of shapes.

To measure the effect of the stretch regularization in a

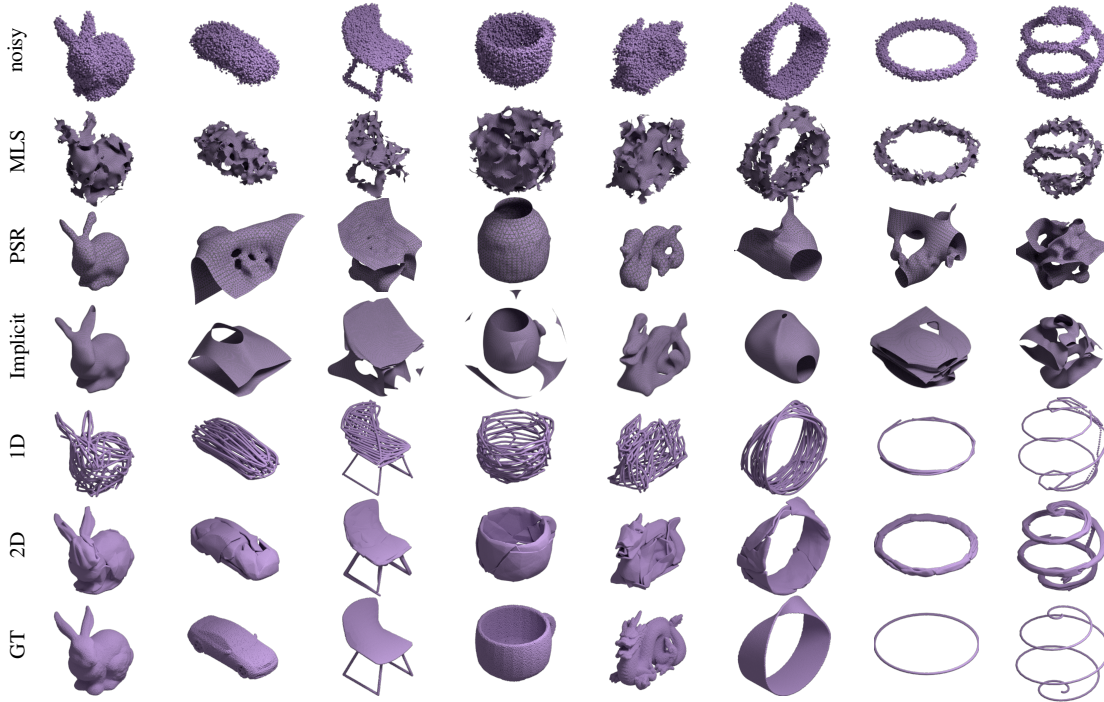


Figure 7: **Qualitative comparison between different denoising methods.** Rows display different methods, whereas columns display different shapes. Baseline methods do not perform as well as the deep manifold prior, even for closed surfaces like the bunny (first column) and the dragon (fifth column). As we can see, 2-manifold parameterizations are better for reconstructing surfaces, whereas 1-manifold counterparts reconstruct the curves (last two columns) more accurately.

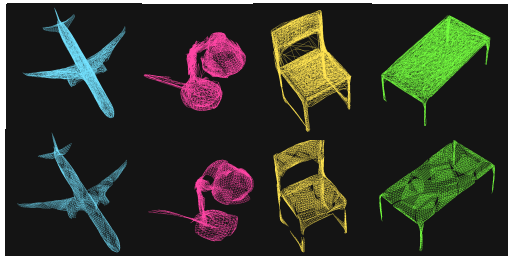


Figure 8: **Autoencoder results.** Results on using AtlasNet [14] trained w/o (top) and w/ (bottom) stretch regularization. The latter results in meshes with reduced deformation and overlap, and removes artifacts where the chair’s back is incorrectly filled.

learning-based scenario, we train a model using the same architecture as AtlasNet [14] on a subset of 50,000 shapes across 13 categories of the ShapeNet dataset [3]. Adding stretch regularization did not significantly impact the Chamfer metric – error of 1.46×10^{-3} and 1.47×10^{-3} with and without regularization. However, the results are qualitatively better. As seen in Figure 8 the regularization reduces the stretch and overlap of the generated surfaces, and eliminates artifacts where holes are incorrectly filled.

We also train a convolutional decoder with stretch regularization on the single-view reconstruction benchmark [7]. Our approach called ConvAtlas is compared against AtlasNet and MRTNet [12] in Table 3. For a fair comparison, we

Architecture	mean/cat.	mean/inst.	#params.
MRTNet	4.80	4.26	81.6M
AtlasNet	4.74	4.38	42.6M
ConvAtlas	4.53	4.00	14.5M

Table 3: **Quantitative results for single-view image-to-shape reconstruction.** The table reports the mean Chamfer distance metric (scaled by 10^3) computed per category and per instance.

use 4K points for evaluation across all methods. ConvAtlas outperforms both approaches in terms of per-category and per-instance error, and also leads to more compact models. Per-category results and experimental details are in the Supplementary material.

6. Conclusion

We presented a manifold prior induced by deep neural networks. Our experiments show that the prior can be effectively used for a variety of manifold reconstruction tasks: denoising, interpolation and single-view reconstruction. Besides, we analyzed the influence of the architecture in the characteristics of the prior by posing the models as GP. In conjunction to the prior induced by deep networks, we showed that using a stretch regularization procedure enables better manifold approximation and improves the quality of the generated meshes, reducing large deformations and overlaps between different parameterizations.

864 **References**

865
866 [1] Panos Achlioptas, Olga Diamanti, Ioannis Mitliagkas, and
867 Leonidas J Guibas. Learning Representations and Generative
868 Models For 3D Point Clouds. In *International Conference on*
869 *Machine Learning*, 2018.
870 [2] Marc Alexa, Johannes Behr, Daniel Cohen-Or, Shachar
871 Fleishman, David Levin, and Claudio T. Silva. Computing
872 and rendering point set surfaces. *IEEE Transactions on visu-*
873 *alization and computer graphics*, 9(1):3–15, 2003.
874 [3] Angel X Chang, Thomas Funkhouser, Leonidas Guibas,
875 Pat Hanrahan, Qixing Huang, Zimo Li, Silvio Savarese,
876 Manolis Savva, Shuran Song, Hao Su, et al. ShapeNet:
877 An information-rich 3D model repository. *arXiv preprint*
arXiv:1512.03012, 2015.
878 [4] Zhiqin Chen and Hao Zhang. Learning implicit fields for
879 generative shape modeling. In *The IEEE Conference on*
880 *Computer Vision and Pattern Recognition*, 2019.
881 [5] Zezhou Cheng, Matheus Gadelha, Subhansu Maji, and
882 Daniel Sheldon. A Bayesian Perspective on the Deep Im-
883 age Prior. In *The IEEE Conference on Computer Vision and*
884 *Pattern Recognition (CVPR)*, 2019.
885 [6] Youngmin Cho and Lawrence K Saul. Kernel methods for
886 deep learning. In *Advances in neural information processing*
887 *systems*, pages 342–350, 2009.
888 [7] Christopher B Choy, Danfei Xu, JunYoung Gwak, Kevin
889 Chen, and Silvio Savarese. 3D-R2N2: A unified approach
890 for single and multi-view 3D object reconstruction. In *Euro-*
891 *pean Conference on Computer Vision*, 2016.
892 [8] Laurent Dinh, David Krueger, and Yoshua Bengio. NICE:
893 Non-linear independent components estimation. *arXiv*
894 *preprint arXiv:1410.8516*, 2014.
895 [9] Haoqiang Fan, Hao Su, and Leonidas Guibas. A Point Set
896 Generation Network for 3D Object Reconstruction from a
897 Single Image. In *IEEE Conference on Computer Vision and*
898 *Pattern Recognition*, 2017.
899 [10] Matheus Gadelha, Subhansu Maji, and Rui Wang. 3d shape
900 generation using spatially ordered point clouds. In *British*
901 *Machine Vision Conference (BMVC)*, 2017.
902 [11] Matheus Gadelha, Subhansu Maji, and Rui Wang. Unsu-
903 pervised 3D Shape Induction from 2D Views of Multiple
904 Objects. In *International Conference on 3D Vision (3DV)*,
905 2017.
906 [12] Matheus Gadelha, Rui Wang, and Subhansu Maji. Mul-
907 ti-resolution Tree Networks for 3D Point Cloud Processing.
908 In *ECCV*, 2018.
909 [13] Kyle Genova, Forrester Cole, Daniel Vlasic, Aaron Sarna,
910 William T Freeman, and Thomas Funkhouser. Learning
911 shape templates with structured implicit functions. In *Inter-*
912 *national Conference on Computer Vision*, 2019.
913 [14] Thibault Groueix, Matthew Fisher, Vladimir G. Kim, Bryan
914 Russell, and Mathieu Aubry. AtlasNet: A Papier-Mâché Ap-
915 proach to Learning 3D Surface Generation. In *Proceedings*
916 *IEEE Conf. on Computer Vision and Pattern Recognition*
917 *(CVPR)*, 2018.
918 [15] Christian Häne, Shubham Tulsiani, and Jitendra Malik. Hi-
919 erarchical surface prediction for 3d object reconstruction. In
920 *International Conference on 3D Vision (3DV)*, 2017.

[16] Michael Kazhdan and Hugues Hoppe. Screened poisson sur-
918 face reconstruction. *ACM Transactions on Graphics (ToG)*,
919 32(3):29, 2013. 920
[17] Durk P Kingma and Prafulla Dhariwal. GLOW: Generative
921 flow with invertible 1x1 convolutions. In *Advances in Neural*
922 *Information Processing Systems*, pages 10236–10245, 2018. 923
[18] Chen-Hsuan Lin, Chen Kong, and Simon Lucey. Learning
924 Efficient Point Cloud Generation for Dense 3D Object Re-
925 construction. In *AAAI Conference on Artificial Intelligence*
926 *(AAAI)*, 2018. 927
[19] Zhaoliang Lun, Matheus Gadelha, Evangelos Kalogerakis,
928 Subhansu Maji, and Rui Wang. 3d shape reconstruction
929 from sketches via multi-view convolutional networks. In *Inter-*
930 *national Conference on 3D Vision (3DV)*, 2017. 931
[20] Lars Mescheder, Michael Oechsle, Michael Niemeyer, Se-
932 bastian Nowozin, and Andreas Geiger. Occupancy networks:
933 Learning 3D reconstruction in function space. In *The IEEE*
934 *Conference on Computer Vision and Pattern Recognition*,
935 2019. 936
[21] Radford M Neal. *Bayesian learning for neural networks*.
937 PhD thesis, University of Toronto, 1995. 938
[22] Zeev Nehari. *Conformal mapping*. Courier Corporation,
939 2012. 940
[23] A Cengiz Öztireli, Gael Guennebaud, and Markus Gross.
941 Feature preserving point set surfaces based on non-linear
942 kernel regression. In *Computer Graphics Forum*, volume 28,
943 pages 493–501. Wiley Online Library, 2009. 944
[24] Jeong Joon Park, Peter Florence, Julian Straub, Richard
945 Newcombe, and Steven Lovegrove. DeepSDF: Learning
946 Continuous Signed Distance Functions for Shape Represent-
947 ation. In *The IEEE Conference on Computer Vision and*
948 *Pattern Recognition*, 2019. 949
[25] Stephan R. Richter and Stefan Roth. Matryoshka Networks:
950 Predicting 3D Geometry via Nested Shape Layers. In *Pro-*
951 *ceedings IEEE Conf. on Computer Vision and Pattern Recog-*
952 *nition (CVPR)*, 2018. 953
[26] Sam T Roweis and Lawrence K Saul. Nonlinear dimen-
954 sionality reduction by locally linear embedding. *science*,
955 290(5500):2323–2326, 2000. 956
[27] Donald Shepard. A two-dimensional interpolation function
957 for irregularly-spaced data. In *Proceedings of the 1968 23rd*
958 *ACM national conference*, pages 517–524. ACM, 1968. 959
[28] Ercan Solak, Roderick Murray-Smith, William E Leithead,
960 Douglas J Leith, and Carl E Rasmussen. Derivative obser-
961 vations in gaussian process models of dynamic systems. In
962 *Advances in neural information processing systems*, 2003. 963
[29] Amir Arsalan Soltani, Haibin Huang, Jiajun Wu, Tejas
964 Kulkarni, and Joshua Tenenbaum. Synthesizing 3d shapes
965 via modeling multi-view depth maps and silhouettes with
966 deep generative networks. In *CVPR*, 2017. 967
[30] Héctor J Sussmann. Orbits of families of vector fields and
968 integrability of distributions. *Transactions of the American*
969 *Mathematical Society*, 180:171–188, 1973. 970
[31] Maxim Tatarchenko, Alexey Dosovitskiy, and Thomas Brox.
971 Multi-view 3D models from single images with a convolu-
972 tional network. In *European Conference on Computer Vision*
973 *(ECCV)*, 2016. 974

972	[32] Maxim Tatarchenko, Alexey Dosovitskiy, and Thomas Brox.	1026
973	Octree generating networks: Efficient convolutional archi-	1027
974	tectures for high-resolution 3d outputs. In <i>IEEE Interna-</i>	1028
975	<i>tional Conference on Computer Vision (ICCV)</i> , 2017.	1029
976	[33] Joshua B Tenenbaum, Vin De Silva, and John C Langford.	1030
977	A global geometric framework for nonlinear dimensionality	1031
978	reduction. <i>science</i> , 290(5500):2319–2323, 2000.	1032
979	[34] Shubham Tulsiani, Tinghui Zhou, Alexei A. Efros, and Ji-	1033
980	tendra Malik. Multi-view supervision for single-view recon-	1034
981	struction via differentiable ray consistency. In <i>Computer Vi-</i>	1035
982	<i>sion and Pattern Recognition (CVPR)</i> , 2017.	1036
983	[35] Dmitry Ulyanov, Andrea Vedaldi, and Victor Lempitsky.	1037
984	Deep image prior. In <i>Proceedings of the IEEE Conference</i>	1038
985	<i>on Computer Vision and Pattern Recognition</i> , 2018.	1039
986	[36] Nanyang Wang, Yinda Zhang, Zhuwen Li, Yanwei Fu, Wei	1040
987	Liu, and Yu-Gang Jiang. Pixel2mesh: Generating 3d mesh	1041
988	models from single rgb images. In <i>ECCV</i> , 2018.	1042
989	[37] Christopher KI Williams. Computing with infinite networks.	1043
990	In <i>Advances in neural information processing systems</i> , pages	1044
991	295–301, 1997.	1045
992	[38] Francis Williams, Teseo Schneider, Claudio Silva, Denis	1046
993	Zorin, Joan Bruna, and Daniele Panozzo. Deep geometric	1047
994	prior for surface reconstruction. In <i>The IEEE Conference on</i>	1048
995	<i>Computer Vision and Pattern Recognition</i> , 2019.	1049
996	[39] Jiajun Wu, Chengkai Zhang, Tianfan Xue, William T Free-	1050
997	man, and Joshua B Tenenbaum. Learning a probabilistic	1051
998	latent space of object shapes via 3D generative-adversarial	1052
999	modeling. In <i>NIPS</i> , 2016.	1053
1000	[40] Yaoqing Yang, Chen Feng, Yiru Shen, and Dong Tian. Fold-	1054
1001	ingNet: Point Cloud Auto-Encoder via Deep Grid Deforma-	1055
1002	tion. In <i>The IEEE Conference on Computer Vision and Pat-</i>	1056
1003	<i>tern Recognition (CVPR)</i> , June 2018.	1057
1004		1058
1005		1059
1006		1060
1007		1061
1008		1062
1009		1063
1010		1064
1011		1065
1012		1066
1013		1067
1014		1068
1015		1069
1016		1070
1017		1071
1018		1072
1019		1073
1020		1074
1021		1075
1022		1076
1023		1077
1024		1078
1025		1079